Acta Cryst. (1997). D53, 513–523

Preliminary Analysis of Amphibian Red Cell M Ferritin in a Novel Tetragonal Unit Cell

YA HA,[a] ELIZABETH C. THEIL[b] AND NORMA M. ALLEWELL[a]*

[a]*Department of Biochemistry, University of Minnesota, St Paul, MN 55108, USA, and* [b]*Department of Biochemistry, North Carolina State University, Raleigh, NC 27695, USA. E-mail: norma@biosci.cbs.umn.edu*

(Received 17 October 1996; accepted 11 March 1997)

Abstract

The ferritins are a multigene family of proteins that concentrate and store iron in all prokaryotic and eukaryotic cells. 24 monomeric subunits which fold as four-helix bundles assemble to form a protein shell with 432 cubic symmetry and an external diameter of ~130 Å. The iron is stored inside the protein shell as a mineralized core ~80 Å in diameter. Recombinant amphibian red cell M ferritin crystallizes in ~2 *M* $(NH_4)_2SO_4$ at pH 4.6 in a space group that has not been reported previously. Electron microscopy, precession photography, Patterson and Fourier maps of the native protein and a UO_2^{2+} derivative, and simulations were used to determine that the unit-cell dimensions are $a = b = 169.6$, $c = 481.2$ Å, $\alpha = \beta = \gamma = 90°$ and the space group is $P4_12_12$ or $P4_32_12$. A preliminary model of the structure was obtained by molecular replacement, with amphibian red cell L ferritin as the model. In contrast to previously determined ferritin crystal structures which have intermolecular contacts at the twofold and threefold molecular axes, M ferritin crystals have a novel intermolecular interaction mediated by interdigitation of the *DE* loops of two molecules at the fourfold molecular axes.

1. Introduction

The ferritins are a family of proteins that sequester and concentrate iron in all cells as a mineralized core within a hollow protein shell that has an external diameter of ~130 Å. The shell has 432 symmetry and is formed by 24 monomeric protein subunits, each of which folds as a four-helix bundle (Theil, 1987, 1990; Harrison *et al.*, 1991). Regulation of iron storage capacity in eukaryotic cells of different organs and at different developmental stages depends on precise control at the levels of transcription, translation and protein function. Amphibia provide a convenient developmental system for studying this regulation and for investigating structure–function relationships.

At least three ferritin subunits are expressed in bullfrog red cells: H, M and L. All three have been cloned, sequenced, expressed in *E. coli* and purified, and are being characterized in terms of the kinetics of iron uptake, oxidation and mineralization by Theil and colleagues (for a recent review, see Waldo & Theil, 1996). H and M ferritins have a high degree of sequence identity (84% in bullfrog red blood cells) and similar functional properties, while L ferritin is more divergent in terms of both primary sequence and function. The sequence differences between H, M and L ferritin subunits are likely to be physiologically relevant, since their expression is tissue specific; for example, in bullfrog liver the ratio of H to M is 1:2, while in red cells the ratio of H, M and L is 6:3:1 (Dickey *et al.*, 1987).

One of the most striking functional differences between H and M ferritins and L ferritin is the rate of oxidation of Fe^{II} to Fe^{III} (Levi *et al.*, 1988); H and M ferritins oxidize Fe^{II} rapidly, while L ferritins oxidize Fe^{II} slowly. Various experimental approaches, including crystallography (Lawson *et al.*, 1991), site-directed mutagenesis (Lawson *et al.*, 1989), Mössbauer spectroscopy (Yang, Meagher, Huynh, Sayers & Theil, 1987; Bauminger, Harrison, Hechel, Nowik & Treffry, 1991), ultraviolet–visible spectroscopy and resonance Raman spectroscopy (Waldo, Ling, Sanders-Loehr & Theil, 1993; Waldo & Theil, 1993) have been used to gain insight into the chemical mechanism of this process.

We have previously determined the structures of recombinant amphibian red cell L ferritin and two mutants under two sets of crystallizing conditions (Trikha *et al.*; 1994, Trikha, Theil & Allewell, 1995) and identified a set of mobile side chains that may be involved in ferritin function. Amphibian red cell H and M ferritins crystallize in a different space group. Since the crystals of H ferritin are more fragile, we have initially emphasized the analysis of the M ferritin crystals. The unit cell is very large, with many weak reflections, making determination of the space group challenging. We have carried out a preliminary analysis of the crystal structure through a combination of electron microscopy, use of a single heavy-atom derivative, simulation of the diffraction pattern and molecular replacement. Our strategy is presented below.

2. Methods

2.1. *Cloning, expression and protein purification*

M ferritin cDNA (Dickey *et al.*, 1987) was subcloned into a PET 3 vector at the *Nde*I site downstream from a

T_4 polymerase promoter which allows proteins translation to begin at the initiator AUG codon. The host cell, *E. coli* BL21 (DE3), encodes the T_7 polymerase under the control of a *lac* operator. Induction with isopropyl-thiogalactoside leads to the synthesis of large amounts of M subunit protein [20–30 mg (liter of culture)$^{-1}$] in the soluble cell fraction. Ferritin was purified by $(NH_4)_2SO_4$ precipitation and fast protein liquid chromatography on a Mono Q column (Pharmacia) as previously described (Waldo *et al.*, 1993).

2.2. *Crystallization of M ferritin and preparation of heavy-metal derivatives*

Crystals were obtained at room temperature by the hanging-drop method by mixing 2 µl of M ferritin protein stock solution at a protein concentration of 17 mg ml^{-1} in 100 m*M* NaMOPS, pH 7.0 with 2 µl of crystallization buffer. The sparse-matrix crystallization conditions of Jancarik & Kim (1991) and a gradient of sodium tartrate from 0.2 to 1.0 *M* were used in the initial search. When small crystals were obtained, generally after several days, a complete factorial search (Carter, 1992) in the vicinity of the initial conditions was carried out. The best crystals were obtained with a crystallization buffer of 100 m*M* $MgCl_2$, 25% $(NH_4)_2SO_4$ and 0.1 *M* sodium acetate at pH 4.6. Most crystals were rod-like with the longest dimension ~1 mm (Fig. 1) and diffracted beyond 2.8 Å.

Heavy-atom derivatives were prepared by washing crystals with the mother liquor and transferring them to solutions of the mother liquor containing a heavy-metal salt at various concentrations. Three heavy-metal derivatives were obtained [$UO_2(NO_3)_2$, $HgCl_2$ and $Sm(Ac)_3$]; of these, $UO_2(NO_3)_2$ produced the largest change in intensities and hence was the one pursued. Cocrystallization was also attempted by adding heavy-metal salts directly to the buffer before mixing it with the protein solution; however, with the exception of $Sm(Ac)_3$ at concentrations <1 m*M*, the heavy-metal salts caused the protein to precipitate.

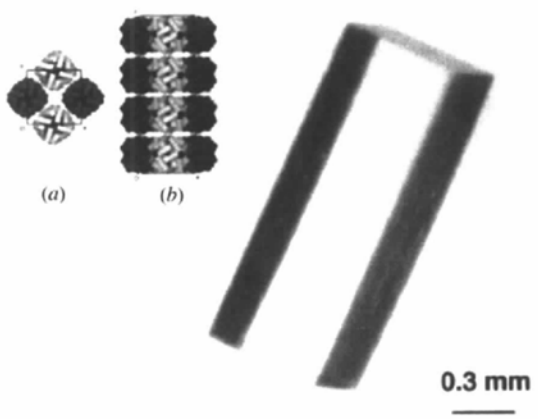

Fig. 1. A typical bullfrog M subunit recombinant ferritin crystal. Insert, the final packing model. Each monomer is represented by a cylinder ~9 Å in diameter and ~50 Å in length. (*a*) View of the (001) plane, (*b*) view of the (010) plane.

2.3. *Precession photography*

10° precession photographs were obtained with a Huber precession camera mounted on a Rigaku RU-200 rotating-anode generator operating at 45 kV and 200 mA. Cu $K\beta$ radiation was eliminated with a nickel filter. The camera distance was 75 mm and the exposure time was 20 h per film.

2.4. *Electron microscopic imaging of the crystal lattice*

A drop of 1% $UO_2(Ac)_2$ in H_2O was added to a drop of a suspension of M ferritin microcrystals in the mother liquor on a carbon-coated grid and blotted immediately with filter paper. Specimens were examined in a Philips CM12 electron microscope using an accelerating voltage of 100 kV with an objective aperture of 40 µm and condenser aperture of 100 µm. The raw images were digitized and the optical diffraction patterns of the lattice calculated using a program written by E. Egelman (University of Minnesota). After the reciprocal lattice had been determined, it was used to filter the raw diffraction pattern and averaged images were obtained by reverse Fourier transform.

2.5. *Data collection*

X-ray diffraction data were collected to 2.8 Å resolution with a Siemens area detector, with the detector distance set to 24 cm and $2\theta = 18°$. Cu $K\alpha$ radiation was generated with a graphite crystal monochromator mounted on a Rigaku RU-200 rotating-anode generator operating at 45 kV and 200 mA. The step size between frames was 0.25°; the collection time for each frame was fixed for each run but adjusted between different runs depending on the crystal size, so that 2 to 3 million counts were acquired for each frame. Most crystals were mounted with the c^* axis parallel to the incident X-ray beam. The software package *ASTRO* (Siemens Energy & Automation, Inc., 1995*a*) was used to design the collection strategy, which varied depending on the orientation of the a^* and b^* axes relative to the incident beam. In general, a φ scan of 100° starting from the angle at which the c^* axis is tangent to the Ewald sphere, plus an ω scan of 50° to fill in the missing region around the a^* axis, samples 99% of the unique reciprocal space from 10 to 3 Å. There was no apparent radiation damage to either native or derivative crystals in 40 h of data collection.

2.6. *Data processing*

Data frames were indexed, integrated, sorted and scaled with the software package *SADIE/SAINT* (Siemens Energy & Automation, Inc., 1995*b*). Data

Table 1. *Data statistics*

The derivative was obtained by soaking M ferritin crystals in 8 m*M* UO_2^{2+} in the crystallization medium.

	Native	Derivative
Space group	$P4_12_12$	Same
Cell dimensions (Å)	$a = b = 169.6$, $c = 481.2$	$a = b = 170.1$, $c = 480.8$
Molecules per unit cell	8	Same
Metal ions	NA	$UO_2(2+)$
Resolution (Å)	2.8	3.0
Number of reflections	151517	153795
Number of unique reflections	98989	76649
$\langle I/\sigma \rangle$	7.4	6.3
R_{sym} (%)*	9.5	13.0
R_{iso} (%)†	NA	21.4
Number of reflections after filtering	23483 (~3.5 Å)	20816

* $R_{sym}(\%) = 100 \times \sum_{hkl} \sum_i |I_{hkl} - \langle I_{hkl} \rangle| / \sum_{hkl} \sum_i I_{hkl}$. I_{hkl} is the recorded intensity and $\langle I_{hkl} \rangle$ is the averaged intensity of the symmetry and Friedel equivalents. † $R_{iso}(\%) = 100 \times \sum_{hkl} |F_{hkl} - F'_{hkl}| / \sum_{hkl} F_{hkl}$. F_{hkl} is the native structure factor and F'_{hkl} is the isomorphous derivative structure factor.

statistics are summarized in Table 1. Reflections along the c^* axis were not well resolved because of the size of the unit cell, crystal mosaicity and the limited camera distance. There are many weak reflections adjacent to strong reflections along this axis and strong reflections spill over into weak reflections during integration because of lack of resolution. When the crystal packing had been determined, the Fourier transform of the packing function was calculated and a filtering process was used to eliminate weak reflections which fell below a defined threshold, as discussed below.

3. Results

3.1. *Precession photography*

*hk*0, 0*kl* and *hhl* sections of the reciprocal lattice are shown in Fig. 2. The unit-cell dimensions indicate that the crystals are tetragonal with minimum unit-cell dimensions of $a = b = 170$ and $c = 240$ Å. (As discussed below, the length of the c axis could not be determined with certainty at this stage.) The *hk*0 section has 4/*mm* symmetry while both 0*kl* and *hhl* sections have *mm* symmetry. Thus, the Laue symmetry is uniquely determined to be 4/*mmm*. All reflections on the a^*, b^* and c^* axes have even indices, consistent with the space group $P4_22_12$.

In the 0*kl* and *hhl* sections, there is a pattern of very weak or missing reflections in certain regions of reciprocal space. This pattern proved crucial in establishing the correct molecular packing. In the 0*kl* section, alternating sets of columns of reflections along the l axis have $l = 2n$ or $2n + 1$ indices (~7 columns per set), while several columns of reflections between these sets appear streaky at this camera distance. Similarly, several columns of reflections in the *hhl* section have only $l = 2n$ indices and the reflections between these columns also appear streaky. These streaky reflections were originally attributed to crystal disorder; however, it later became apparent that they were simply poorly resolved as a

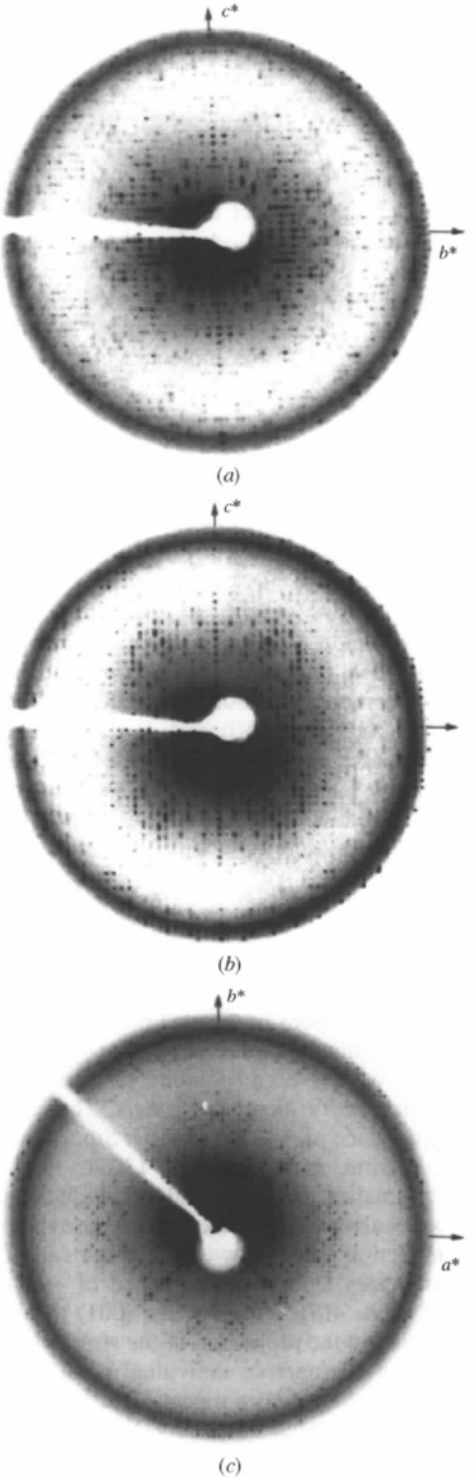

Fig. 2. 10° precession photographs. (*a*) 0*kl*, (*b*) *hhl* and (*c*) *hk*0 sections. Reciprocal axes a^*, b^* and c^* are marked.

result of crystal mosaicity, their close spacing and the camera distance. Reflections in the *hk*0 section are all well resolved.

3.2. *Self-rotation function*

To determine the orientation of the molecular axes, the self rotation function (Rossmann & Blow, 1962) was calculated, using the program *POLARRFN* written by W. Kabsch as implemented in the *CCP*4 package (Collaborative Computational Project, Number 4, 1994). Sections $\kappa = 180$, 120 and 90° are shown in Fig. 3. These results indicate that one of the molecular fourfold axes is parallel to the crystallographic 4_2 screw axis while the other two molecular fourfold axes lie on the face diagonals of the *ab* plane. The angular relationship of the molecular fourfold, threefold and twofold rotation axes is consistent with the molecular 432 symmetry of ferritins.

3.3. *Preliminary model*

Given the twofold rotation axis generated by the crystallographic 4_2 screw axis, the fact that there is only one molecular fourfold axis in this direction, and the relative sizes of the ferritin molecule and the unit cell, the crystallographic twofold axis and the molecular fourfold axis must coincide. One possible packing of molecules in this unit cell is with the centers of the molecules at special positions *A* (0.00, 0.00, 0.00), *B* (0.50, 0.50, 0.00), *C* (0.00, 0.00, 0.50) and *D* (0.50, 0.50, 0.50), with each molecule incorporating the crystallographic 222 symmetry into its molecular 432 symmetry. In the initial model, molecules of tadpole L ferritin (Trikha *et al.*, 1994) were placed at each of these positions.

3.4. *Electron microscopy*

Two negatively stained electron micrographs of the crystal lattice are shown in Fig. 4. Also shown are comparable projections of the electron density calculated from the preliminary model. Figs. 4(*a*)–4(*c*) show the (010) plane, a view corresponding to the projection of the electron density along the *y* axis. There is a clear repeating distance of ~120 Å along *z*. Since the diameter of other ferritin molecules is ~130 Å, this distance is slightly smaller than expected. Individual molecules cannot be resolved along the *x* axis because they overlap at this projection angle. However, the optical diffraction pattern indicates a repeating distance of ~85 Å along the *x* axis. Figs. 4(*d*)–4(*f*) show the (001) plane, a view corresponding to the projection of the structure down the *z* axis. In the micrograph, individual molecules can be seen to pack tightly with a repeating distance of 120 Å, in good agreement with the model. While the resolution of the electron micrographs limits further analysis, it is apparent that there are no packing defects and that the molecules are tightly packed in all three dimensions.

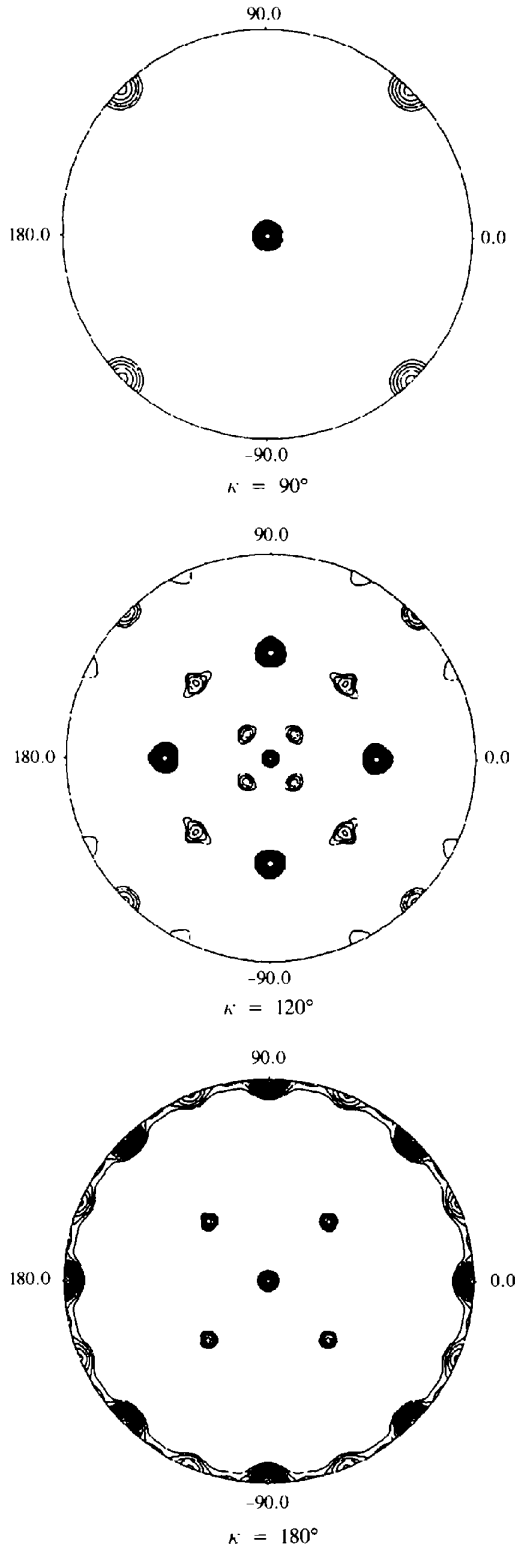

Fig. 3. Self-rotation function with $\kappa = 90$, 120 and 180° for structure factors in the 10–3.5 Å resolution range with amplitudes between 2 and 20. Patterson search vectors from 20 to 60 Å were used in the calculation.

3.5. *Native Patterson map*

There are three well resolved Patterson peaks near positions *B*, *C* and *D*, consistent with the assumption that molecules are stacked on top of each other along the *c* axis and there is one molecule positioned close to the center of *ab* plane. However, while the model predicts Patterson peaks at fractional coordinates (0.50, 0.50, 0.00), (0.00, 0.00, 0.50), (0.50, 0.50, 0.50), the three peaks are at fractional coordinates (0.037, 0.037, 0.500), (0.500, 0.500, 0.036) and (0.463, 0.463, 0.464), ~8.9, 8.6 and 12.4 Å, respectively, from the special positions with 222 point-group symmetry.

3.6. *Heavy-atom derivative and difference Fourier maps*

At this point, we considered the possibility that the M ferritin structure might differ substantially from the starting model or that the molecular symmetry might be altered due to crystal packing. Since solving such a structure would require multiple isomorphous replacement, a UO_2^{2+} derivative was prepared and data from the derivative were used to calculate difference Patterson and difference Fourier maps, with phases still based on the preliminary model. These maps revealed a metal binding site on the surface of the molecule at position *A*. In the second difference Fourier map based on SIR (single isomorphous replacement) phases calculated from the first site, four new sites were found on the surface of the molecule at position *C* in the preliminary model. These four sites, ~13 Å apart, are related by a local fourfold rotation axis parallel to the *c* axis, the center of which corresponds to the UO_2^{2+} site on molecule *A* (Fig. 5). Since there is neither local fourfold nor crystallographic fourfold axis at this point, the splitting into four sites can only be explained by an error in the original space-group assignment.

3.7. *Revised model*

At this point, we used the preliminary model to calculate the diffraction pattern and found that the simulated pattern did not have the unusual features of the precession photographs. However, simulations in which one molecule along the *c* axis was offset relative to another molecule by a small translation vector had both the pattern of odd and even reflections and the streaks seen in the precession photographs (see below). The possibility of a 4_1 or 4_3 screw axis along the *c* axis was then considered. The smallest cell that will accommodate a 4_1 or 4_3 screw axis and ferritin molecules with reasonable contacts has to have a *c* axis twice as large as in the initial model. Hence, the data were reindexed as $P4_12_12$ with $a = b = 169.6$, $c = 481.2$ Å, processed (see below), and used to recalculate the Patterson map. The highest peaks are listed in Table 2, from which the center of the ferritin molecule is calculated to be at fractional coordinates (0.036, 0.000, 0.384). Since 4_1 and 4_3 screw axes cannot be differentiated when

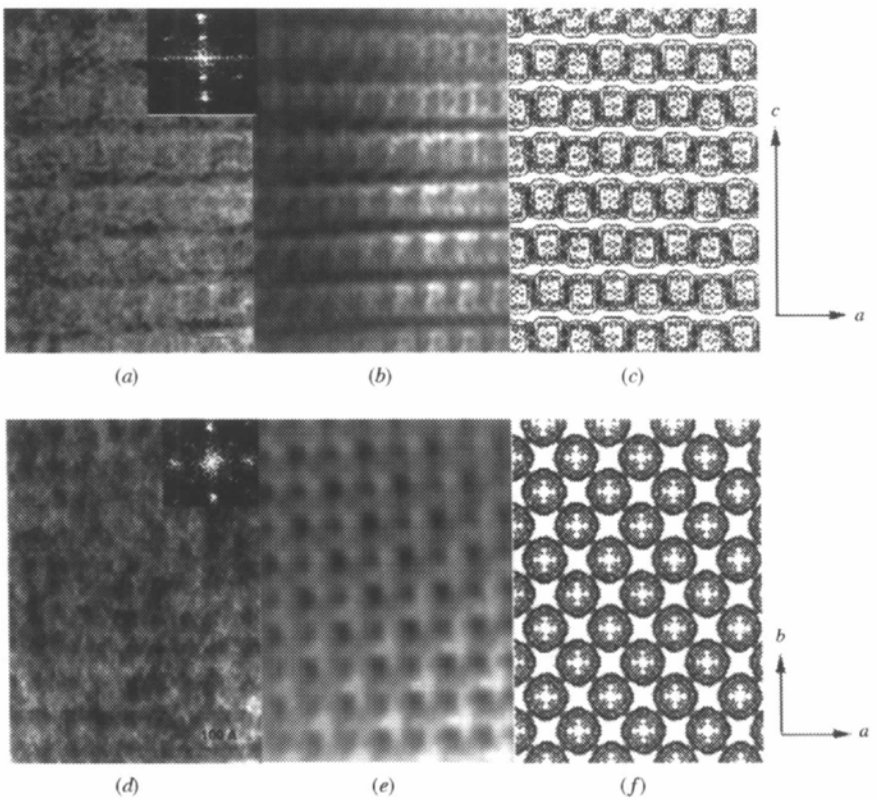

Fig. 4. Electron micrographs of crystals negatively stained with $UO_2(Ac)_2$ magnified 125 000×. (*a*) Raw image of the (010) plane; insert, optical diffraction of this image, (*b*) filtered image, (*c*) calculated projection of the electron density on the (010) plane, (*d*) raw image of the (001) plane; insert, optical diffraction of this image, (*e*) filtered image, (*f*) calculated projection of the electron density on the (001) plane.

the non-crystallographic fourfold axis is parallel to the crystallographic fourfold screw axis (Ha & Allewell, 1997), we arbitrarily based our model on the space group $P4_12_12$.

3.8. *Simulations*

Since the combination of the molecular fourfold and twofold rotation axes with parallel crystallographic 4_1 and twofold rotation axes produces a pure translation symmetry element, the packing can be treated as a convolution of one ferritin molecule with a delta function that defines the origin of each molecule. The Fourier transform of a model of the M ferritin molecule in a unit cell with $P1$ symmetry is shown in Figs. 6(*d*)–6(*f*). The Fourier transform of the delta function (Figs. 6*a*–6*c*) with non-zero values at the centers of the molecules in the unit cell defined above produces a diffraction pattern with the distinctive pattern of odd and even reflections and streaks observed in the experimental data. When the molecular transform is multiplied by the transform of this delta function, these features are preserved and the result is almost identical to that recorded by precession photography (Figs. 6*g*–6*i*).

Table 2. *Major peaks in native Patterson, calculated with reflections within the resolution range 10.0–3.5 Å*

Peak index	*x* (fractional)	*y* (fractional)	*z* (fractional)	Peak height (σ)
1	0.000	0.000	0.000	364
2	0.500	0.500	0.018	180
3	0.000	0.073	0.500	77
4	0.037	0.037	0.250	70
5	0.428	0.500	0.482	27
6	0.464	0.464	0.232	27
7	0.463	0.463	0.268	26

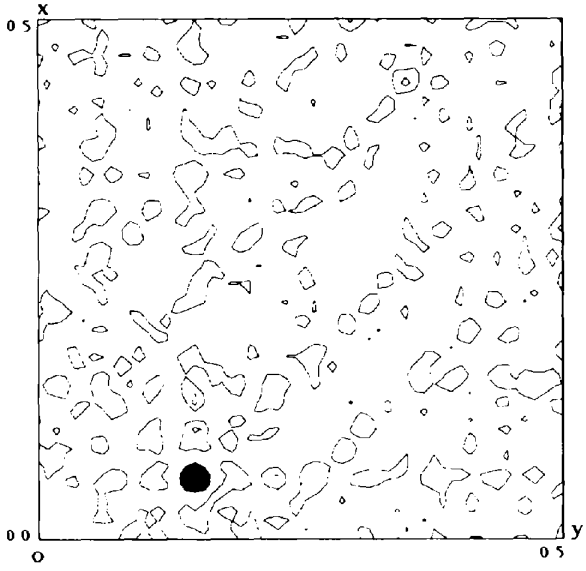

(*a*)

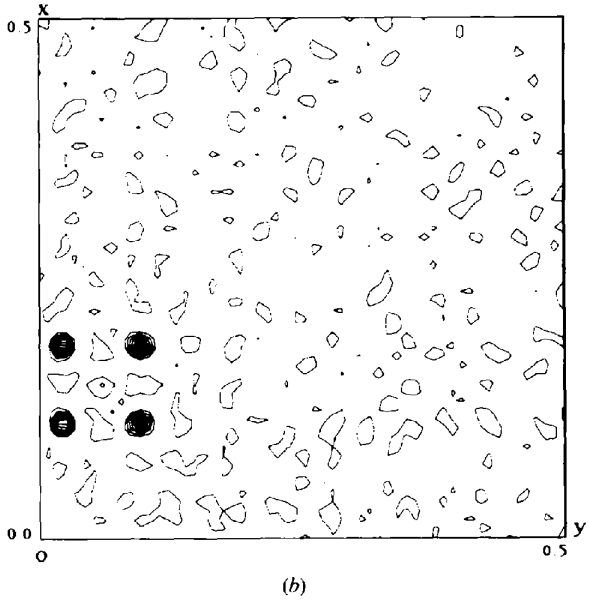

(*b*)

Fig. 5. Difference Fourier map calculated with SIR phases. (*a*) The first site, with fractional coordinates (0.061, 0.150, 0.160); (*b*) Four additional sites, with fractional coordinates (0.186, 0.026, 0.340), (0.186, 0.097, 0.340), (0.115, 0.026, 0.340) and (0.115, 0.097, 0.340), and their center at (0.151, 0.061, 0.340).

3.9. *Packing transforms*

The observed diffraction pattern can be predicted mathematically. In a simpler case, $P4_1$, the transform of the delta function can be written as

$$F_{hkl} = \exp(2\pi ihx) + \exp[2\pi i(kx + l/4)] + \exp[2\pi i(-hx + l/2)] + \exp[2\pi i(-kx + 3l/4)],$$

where the delta function assumes non-zero value only at fractional coordinates (x, 0, 0), (0, x, 1/4), ($-x$, 0, 1/2) and (0, $-x$, 3/4).

In the 0kl section,

$$\begin{aligned} F_{0kl} &= 1 + \exp[2\pi i(kx + l/4)] + \exp(l\pi i) + \exp[2\pi i(-kx + 3l/4)] \\ &= 2 + \exp(2\pi ikx) + \exp(-2\pi ikx) \\ &= 2 + 2\cos 2\pi kx \qquad (l = 4n) \\ &= 2 - 2\cos 2\pi kx \qquad (l = 4n + 2) \\ &= 2\sin 2\pi kx \qquad (l = 4n + 1,\ 4n + 3) \end{aligned}$$

For reflections with l indices $4n$ or $4n + 2$, the maximum intensity is four times the intensity of reflections with l indices $4n + 1$ or $4n + 3$. The periodicity along the k axis is $1/x$ for $4n$ or $4n + 2$ reflections, and $1/2x$ for $4n + 1$ or $4n + 3$ reflections. Since the intensities of the $4n$ and $4n + 2$ reflections are out of phase by 180°, a pattern of alternating indices along the l axis is produced. For $4n + 1$ and $4n + 3$ reflections, the maximum is at the position when both $4n$ and $4n + 2$ reflections are non-zero and relatively weak. This produces the apparent

streakiness since the reflections are more closely spaced and weaker than those in regions where either $4n$ or $4n+2$ reflections dominate (Fig. 7*a*).

In the *hhl* section,

$$\begin{aligned} F_{hhl} &= \exp(2\pi i hx) + \exp[2\pi i(hx + l/4)] \\ &\quad + \exp[2\pi i(-hx + l/2)] + \exp[2\pi i(-hx + 3l/4)] \\ &= 4\cos 2\pi hx \qquad (l = 4n) \\ &= 2\sin 2\pi hx(-1 + i) \qquad (l = 4n + 1) \\ &= 0 \qquad (l = 4n + 2) \\ &= 2\sin 2\pi hx\ (1 + i) \qquad (l = 4n + 3). \end{aligned}$$

Again, the dominant feature in this section is that the $4n$ reflections are twice as strong as those with $l = 4n + 1$ and $4n + 3$ and all $4n + 2$ reflections have zero intensity. The $4n$ and $4n + 1$ or $4n + 3$ reflections also produce a pattern of streakiness similar to that of the $0kl$ section. The periodicity of the $4n$ reflections is $1/2x$. The band of discrete strong reflections is about 1.4 times wider than in the $0kl$ section (Fig. 7*b*).

From the above analysis, it is apparent that the position of each molecule relative to the 4_1 screw axis (fractional coordinate x) can be estimated independently by inspecting the pattern of strong reflections in $0kl$ or *hhl* precession photographs. Observing where the strong reflections change from indices $4n$ to $4n + 2$ in the $0kl$ section and where the $4n + 1$ and $4n + 3$ reflections merge in both $0kl$ and *hhl* sections (streaky reflections) in a series of simulations in which x is varied yields the same value for x as that obtained by Patterson map analysis or the translation function discussed below.

3.10. *Data filtering*

The close spacing of reflections along the l axis ($\sim 0.2°$) creates an artifact in the area detector data that can be demonstrated by comparing the reconstruction of the weighted reciprocal lattice with the actual image recorded on the precession photographs. As shown, in the reconstructed reciprocal lattice in Fig. 8(*a*), there appear to be consecutive 'strong reflections' along the l axis. However, the $0kl$ section of the precession photograph shows that only reflections with $l = 4n + 2$ are strong in this region. This inconsistency is the result of attempts to integrate reflections in a data frame that has limited resolution at this camera distance. Since many strong reflections are separated by several weak reflections along the l axis as a result of the molecular packing, a reasonable data set can still be obtained from the raw intensities by filtering out the instrumental artifacts.

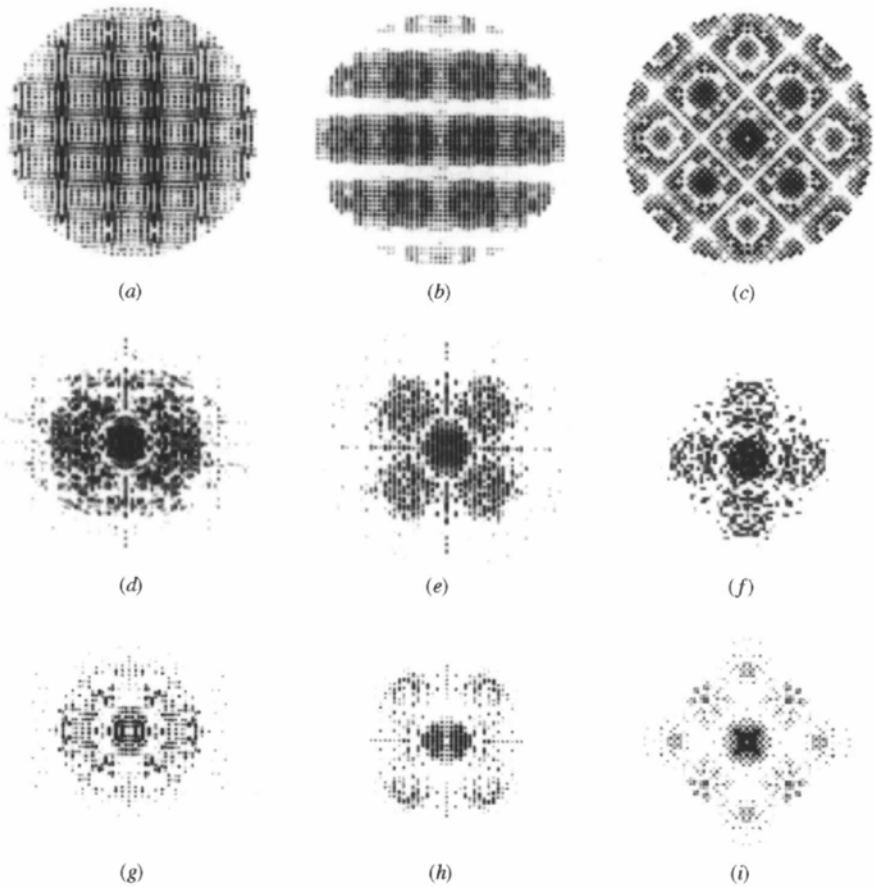

Fig. 6. Sections (*a–c*): Fourier transforms of the packing delta function as discussed in the text; (*a*) $0kl$ section, (*b*) *hhl* section, (*c*) $hk0$ section. Sections (*d–f*): Fourier transforms of the M ferritin model in a $P1$ cell; (*d*) $0kl$ section, (*e*) *hhl* section, (*f*) $hk0$ section. Sections (*g–i*): the products of the Fourier transforms of the delta function and M ferritin model, (*g*) $0kl$ section, (*h*) *hhl* section, (*i*) $hk0$ section. Note the similarity of (*g*)–(*i*) to the corresponding sections in Fig. 2.

As discussed above, the structure factor is the product of the transform of the molecule and that of a packing delta function, and the amplitudes of most reflections should be low where the amplitudes of the transform of the packing function are low. The Fourier transform of this delta function can therefore be used to filter out weak reflections which have significant contributions in the original data set from nearby strong reflections.

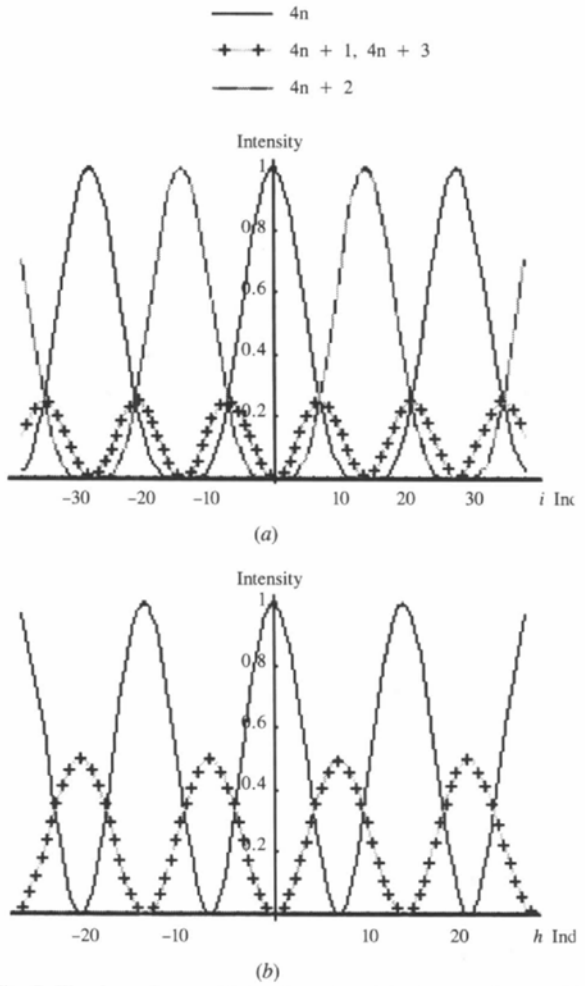

Fig. 7. The dependence of intensities of the Fourier transforms of the packing delta function on the k index with $x = 0.036$ in (*a*) $0kl$ section; (*b*) hhl section.

As shown in Figs. 8(*b*)–8(*c*), the filtering procedure improves the consistency between the area-detector data and the film.

3.11. *Molecular replacement*

To confirm the results obtained so far, cross-rotation and translation functions as implemented in *X-PLOR* (Brünger, 1992) were calculated with a model of M ferritin based on tadpole L ferritin (Trikha *et al.*, 1994) and rotated 45° around the c axis (Table 3). The three highest cross-rotation peaks are related by the molecular threefold rotation axis and correspond to the orientation obtained by the self-rotation function. This orientation was optimized by Patterson correlation rigid-body refinement (Brünger, 1990) and the refined model was then used for a translation search. The translation function is shown in Fig. 9 and the highest peaks are listed in Table 4. They correspond to positions ~6.4 Å from the crystallographic 4_1 screw axis and ~4.3 Å from the 2_1 screw axis, respectively, and confirm the conclusions drawn from the Patterson peak analysis and simulations described above. When the model was subjected to rigid-body refinement, the electron-density map was clearly interpretable (Fig. 10).

3.12. *Molecular contacts*

The ferritin molecules in this space group interact with each other through residues in the loops between D and E helices at the fourfold molecular axis (Fig. 11). The offset of ferritin molecules along the fourfold axis by 9 Å allows one of the four loops of one molecule to fit into the fourfold channel of the adjacent molecule. Left- and right-handed screw axes cannot be distinguished by pure inspection of the chemical contact, since the loops are symmetrically related.

4. Discussion

The quaternary structures of ferritins are well conserved, [Clegg, Stansfield, Bourne & Harrison, 1980; Thomas *et al.*, 1988; Lawson *et al.*, 1991; Trikha *et al.*, 1994; Frolow, Kalb (Gilboa) & Yariv, 1994] and ferritins frequently crystallize in the space group $F432$ with unit-cell dimensions of $a = b = c \simeq 183$ Å, one monomer per asymmetric unit and the crystallographic 432 symmetry

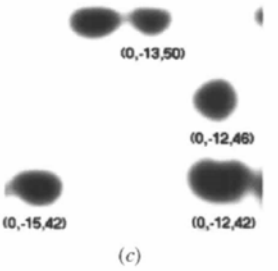

Fig. 8. The reconstructed diffraction intensity from area-detector data before and after 'filtering'. The filtering process improves the agreement between the final data set and precession photographs. (*a*) Unfiltered data, (*b*) filtered data, (*c*) the corresponding region recorded by precession photography.

Table 3. *Cross-rotation function*

The M ferritin model was based on bullfrog L ferritin PDB coordinates (Trikha *et al.*, 1994) with a rotation of 45° around the *c* axis. Thus, the first peak corresponds to this orientation and is consistent with the self-rotation function. Indices 10 and 13 correspond to 120° rotation about the molecular threefold axis.

Index	θ1 (°)	θ2 (°)	θ3 (°)	RF value*
1	0.00	0.00	0.00	1.81
10	45.00	90.00	45.00	1.69
13	314.78	90.00	315.22	1.66
170	32.50	0.00	32.50	0.44
178	12.50	0.00	12.50	0.44
194	134.94	90.00	113.34	0.42

* RF value is defined as the product of rotated vectors of the model Patterson map and the interpolated values of the observed Patterson map.

incorporated into the molecular symmetry. The main intermolecular interaction is through two divalent metal ions, either Cd^{2+} or Ca^{2+}, which are chelated by conserved or engineered Asp and Gln residues at the twofold molecular axis (Lawson *et al.*, 1991). Native human H ferritin, which has a sequence in this region similar to that of bullfrog M ferritin (QDIKK), has not been crystallized in the space group *F*432 (Lawson *et al.*, 1991). Several other crystal forms of horse-spleen ferritins have been reported (Harrison, 1963; Hoy, Harrison & Hoare, 1974) and two of these structures have been solved. The space group of one crystal form is $P42_12$ with $a = b = 147$ and $c = 153$ Å and two ferritin molecules per cell, each incorporating the crystallographic fourfold rotation axis into the molecular symmetry (Granier, Gallois, Dautant, Langlois d'Estaintot & Précigoux, 1996). The other molecular fourfold forms an angle of ~23°

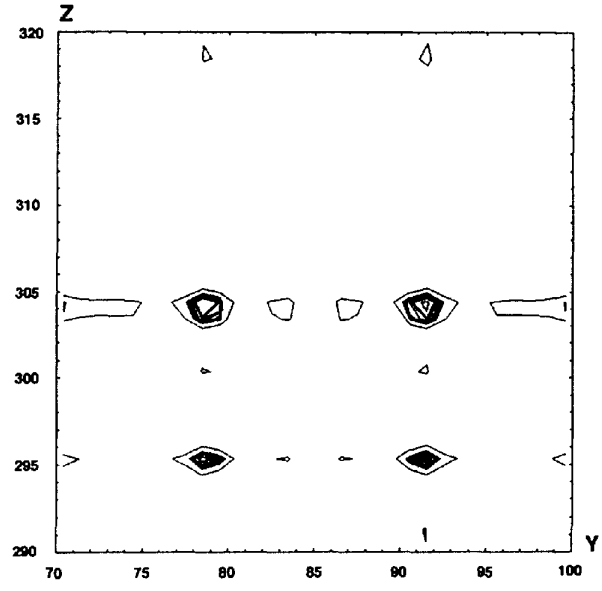

Fig. 9. Section of the translation function is shown for $70 < y < 100$ Å and $290 < z < 320$ Å. The four highest peaks are about 8 Å away from the special position (0.0, 0.5, 0.625).

Table 4. *The highest peaks in the translation function*

The mean of the *T* function is 0.157 with a σ of 0.018. The four peaks with magnitudes of ~ 5σ differ only in the choice of origin.

Index	*x* (fractional)	*y* (fractional)	*z* (fractional)	*T*-function value*
1	0.000	0.462	0.633	0.272
2	0.000	0.538	0.615	0.270
3	0.000	0.462	0.615	0.254
4	0.000	0.538	0.633	0.253

* The *T*-function value is defined as the correlation between $E^2_{obs}(hkl)$ and $E^2_{calc}(hkl)$.

with the crystallographic twofold axis. A salt bridge involving a metal ion coordinated by a Thr and a Glu of one molecule and a Glu and a Gln of another forms the intermolecular contacts. The space group of the second crystal form is $P2_12_12$ with $a = 182$, $b = c = 129$ Å (Langlois d'Estaintot *et al.*, 1996). It can be considered to be derived from *F*432 by a ~6° rotation around the *c* axis, perhaps as a result of the presence of Pt-mesoporphyrin IX. Intermolecular contacts are *via* two metal ions coordinated by Asp and Gln on the twofold molecular axis.

Several crystal forms have been reported for bacterioferritins [Smith, Ford, Harrison, Yariv & Kalb (Gilboa), 1989] and one structure has been solved (Frolow *et al.*, 1994). The packing is approximately body centered *I*432 with $a = b = c \simeq 147$ Å. The final structure was solved in a slightly different form, $P4_22_12$, with $a = b \simeq 210$, $c \simeq 145$ Å and a unit cell twice as large.

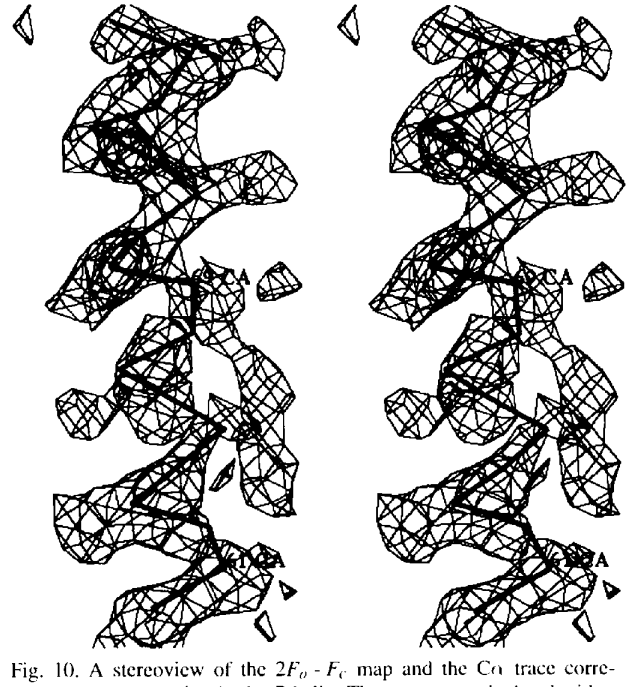

Fig. 10. A stereoview of the $2F_o - F_c$ map and the Cα trace corresponding to a region in the *B* helix. The map was calculated with a M ferritin model generated from L ferritin coordinates and subjected to rigid-body refinement and the map cutoff was set to 1σ.

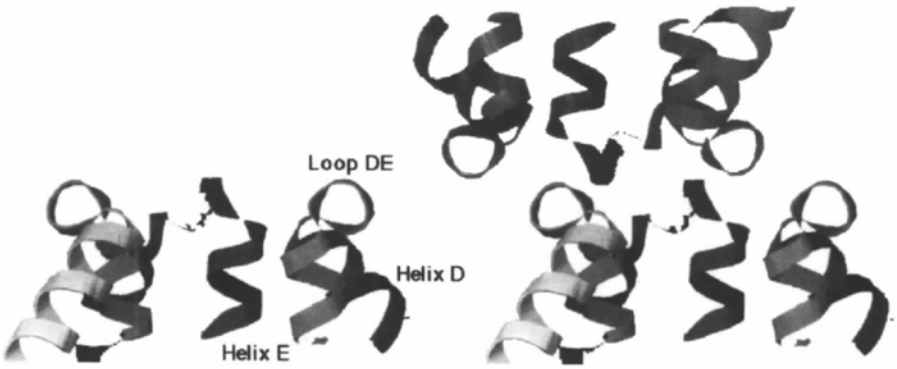

Fig. 11. Ribbon diagram of the crystal contact region along the fourfold screw axis. (*a*) A single molecule; (*b*) the same molecule in contact with a second molecule.

The crystal contact region is at the threefold molecular axis. In this report, we have described another crystal form of ferritin in the tetragonal space group $P4_12_12$. To a first approximation, the packing is simply $P432$ with $a = b = c \simeq 120$ Å with one molecule per cell and each ferritin molecule making contacts with other molecules through the fourfold molecular axis. However, the unit cell is distorted at every molecular contact to generate screw axes along every fourfold axis. The screw axis may result from steric constraints, van der Waals, ionic interactions, and global electrostatic effects (Takeda, Yoshimura, Endo, Takahashi & Nagayama, 1995). Since the sequence of human H ferritin in the *DE* loop (GAPESG) is similar to that of bullfrog M ferritin (GLPENG) and the human H K86Q mutant favors the $F432$ crystal form, it seems likely that the crystal contacts in the space group $P4_12_12$ are weaker than those produced by the double salt bridge. However, in the absence of the divalent metal ion mediated salt bridge, H and M ferritins stack at the fourfold axes to adopt a sterically favored docking position, which then favors a slight offset of molecular symmetry axes from the crystallographic symmetry axes.

H and M amphibian ferritins crystallize under a wide variety of solution conditions, with various precipitating reagents (ammonium sulfate, sodium tartrate, sodium formate, lithium sulfate, polyethylene glycols with a range of molecular weights), with various divalent metal ions, *e.g.* Mg^{2+} and Cd^{2+}, and at different pHs from 4 to 8. These crystals have similar morphologies and several have been shown to have very similar diffraction patterns, suggesting that they have crystallized in the same space group with identical crystal contacts. Thus, interactions along the fourfold molecular axis represent a general mode of interaction between different molecules of amphibian H and M ferritins, which may have implications for intermolecular 'communication' *in vivo*. To solve this packing problem, we have separated the packing term from the molecular term using convolution and transform theory. This approach may be useful in other cases when the molecule of interest has high symmetry and different molecules in the unit cell are related by translation elements. In our study of M ferritin crystals, the unique features of the diffraction pattern in low-resolution precession photographs provided us with crucial information about the molecular packing. We are currently refining the M ferritin model with the filtered data; we are also investigating the possibility of obtaining higher quality data through the use of focusing mirrors or a synchrotron beamline and a longer crystal-to-detector distance. However, the quality of the data may be ultimately limited by the mosaicity of the crystal, since the angular separation of individual reflections from these crystals is only 0.2°. Regardless of the data used in the refinement, we expect the refined structure to provide new information about the intermolecular contacts, structural differences between M ferritin and other ferritins and the relationship of these differences to ferritin function.

This work was supported by NIH grants DK-50727 (to NMA) and DK-20251 (to ECT). Diffraction data were collected at the Kahlert Center for Structural Biology at the University of Minnesota; the electron micrographs were obtained at the Minnesota Agricultural Experiment Station. Some intensive calculations were carried out on a Cray X-MP EA at the University of Minnesota Supercomputer Institute. We would like to thank T. Schagat for subcloning the bullfrog ferritin M subunit in the protein expression vector, D. Danger for purifying the proteins, Drs L. Banaszak and D. Ohlendorf for facilitating our use of the diffraction equipment and helpful discussions, G. Ahlstrand for help with the electron microscopy and Dr E. Egelman for help with image processing.

References

Bauminger, E. R., Harrison, P. M., Hechel, D., Nowik, I. & Treffry, A. (1991). *Biochim. Biophys. Acta*, **1118**, 48–58.
Brünger, A. T. (1990). *Acta Cryst.* A**46**, 46–57.
Brünger, A. T. (1992). *X-PLOR manual, Version* 3.0, New Haven, CT, USA.

Carter, C. W. Jr (1992). *Crystallization of Nucleic Acid and Proteins, A Practical Approach*, edited by A. Ducruix & R. Giegé, ch. 3, 47–71. Oxford University Press.

Clegg, G. A., Stansfield, R. F. D., Bourne, P. E. & Harrison, P. M. (1980). *Nature (London)*, **288**, 298–300.

Collaborative Computational Project, Number 4 (1994). *Acta Cryst.* D**51**, 760–763.

Dickey, L. F., Sreedharan, S., Theil, E. C., Didsbury, J. R., Wang, Y. H. & Kaufman, R. E. (1987). *J. Biol. Chem.* **262**, 7901–7907.

Frolow, F., Kalb (Gilboa), A. J. & Yariv, J. (1994). *Nature Struct. Biol.* **1**, 453–460.

Granier, T, Gallois, B., Dautant, A., Langlois d'Estaintot, B. & Précigoux, G. (1996). *Acta Cryst.* D**52**, 594–596.

Ha, Y. & Allewell, N. M. (1997). In the press.

Harrison, P. M. (1963). *J. Mol. Biol.* **6**, 404–422.

Harrison, P. M., Andrews, S. C., Artymiuk, P. J., Ford, G. C., Guest, J. R., Hirzmann, J., Lawson, D. M., Livingstone, J. C., Smith, J. M. A., Treffry, A. & Yewdall, S. J. (1991). *Adv. Inorg. Chem.* **36**, 449–486.

Hoy, T. G., Harrison, P. M. & Hoare, R. J. (1974). *J. Mol. Biol.* **86**, 301–308.

Jancarik, J. & Kim, S.-H. (1991). *J. Appl. Cryst.* **24**, 409–411.

Langlois d'Estaintot, B., Dautant, A., Granier, T., Gallois, B., Michaux, M. & Précigoux, G. (1996). *Acta Cryst.* D**52**, 597–600.

Lawson, D. M., Artymiuk, P. J., Yewdall, S. J., Smith, J. M. A., Livingstone, J. C., Treffry, A., Luzzago, A., Levi, S., Arosio, P., Cesareni, G., Thomas, C. D., Shaw, W. V. & Harrison, P. M. (1991). *Nature (London)*, **349**, 541–544.

Lawson, D. M., Treffry, A, Artymiuk, P. J., Harrison, P. M., Yewdall, S. J., Luzzago, A., Cesareni, G., Levi, S. & Arosio, P. (1989). *FEBS Lett.* **254**, 207–210.

Levi, S., Luzzago, A., Cesareni, G., Cozzi, A., Franceschinelli, F., Albertini, A. & Arosio, P. (1988). *J. Biol. Chem.* **253**, 4451–4458.

Rossmann, M. G. & Blow, D. M. (1962). *Acta Cryst.* **15**, 24–31.

Siemens Energy & Automation, Inc. (1995*a*). *ASTRO Manual.* 6300 Enterprise Lane, Madison, WI 53719–1173, USA.

Siemens Energy & Automation, Inc. (1995*b*). *SADIE/SAINT Manual.* 6300 Enterprise Lane, Madison, WI 53719–1173, USA.

Smith, J. M. A., Ford, G. C., Harrison, P. M., Yariv, J. & Kalb (Gilboa), A. J. (1989). *J. Mol. Biol.* **205**, 465–467.

Takeda, S., Yoshimura, H., Endo, S., Takahashi, T. & Nagayama, K. (1995). *Proteins*, **23**, 548–556.

Theil, E. C. (1987). *Ann. Rev. Biochem.* **56**, 289–315.

Theil, E. C. (1990). *Adv. Enzymol. Rel. Areas Mol. Biol.* **63**, 421–449.

Thomas, C. D., Shaw, W. V., Lawson, D. M., Treffry, A., Artymiuk, P. J. & Harrison, P. M. (1988). *Biochem. Soc. Trans.* **16**, 838–839.

Trikha, J., Theil, E. C. & Allewell, N. M. (1995). *J. Mol. Biol.* **248**, 949–967.

Trikha, J., Waldo, G. S., Lewandowski, F. A., Ha, Y., Theil, E. C., Weber, P. C. & Allewell, N. M. (1994). *Proteins*, **18**, 107–118.

Waldo, G. S., Ling, J., Sanders-Loehr, S. & Theil, E. C. (1993). *Science*, **259**, 796–798.

Waldo, G. S. & Theil, E. C. (1993). *Biochemistry*, **32**, 13261–13269.

Waldo, G. S. & Theil, E. C. (1996). *Comprehensive Supermolecular Chemistry, Supermolecular Reactivity and Transport*, Vol. 5, edited by K. Suslick, pp. 65–89. Oxford: Pergamon Press.

Yang, C.-Y., Meagher, A., Huynh, B. H., Sayers, D. E. & Theil, E. C. (1987). *Biochemistry*, **26**, 497–503.